On the relation between gravity waves and wind speed in the lower stratosphere over the Southern Ocean

Riwal Plougonven*, Alvaro de la Cámara†, Valérian Jewtoukoff, Albert Hertzog and François Lott.

Laboratoire de Météorologie Dynamique, Ecole Polytechnique, Palaiseau 91128, France.

Corresponding author address: Riwal Plougonven, Laboratoire de Météorologie Dynamique, Ecole Polytechnique, Palaiseau 91128, France.

E-mail: riwal.plougonven@polytechnique.org

†Current affiliation: National Center for Atmospheric Research, Boulder, Colorado, U.S.A.

ABSTRACT

The relationship between gravity wave momentum fluxes and local wind speed is investigated for oceanic regions at high Southern latitude during austral spring. The motivation is to better describe the gravity wave field, by identifying a simple relationship between gravity waves and the large-scale flow. The tool used to describe the gravity waves are probability density functions of the gravity wave momentum fluxes. Three independent datasets covering high latitudes in the Southern Hemisphere springtime are analyzed: simulations with a mesoscale model, analyses from the European Center for Medium-Range Weather Forecasts and observations from superpressure balloons of the Concordiasi campaign in 2010. A remarkably robust relation is found, with stronger momentum fluxes much more likely in regions of strong winds. The tails of the probability density functions are well described as lognormal. The median momentum flux increases linearly with background wind speed: for winds larger than 50 $\mathrm{m\,s^{-1}}$, the median gravity wave momentum fluxes are about 4 times larger than for winds weaker than 10 $\mathrm{m\,s^{-1}}$. From model output, this relation is found to be relevant from the tropopause to the mid-stratosphere at least, and to increase somewhat with height. Several different processes contribute to this relation, involving both the distribution of sources and the effects of propagation and filtering. It is argued that the location of tropospheric sources is the main contributor in the upper-troposphere and lowermost stratosphere, and that lateral propagation into regions of strong winds becomes increasingly important above.

1. Introduction

Internal gravity waves constitute a ubiquitous component of atmospheric motions, with horizontal scales ranging from a few kilometers to more than a thousand kilometers (Fritts and Alexander 2003). These scales imply that at least some of their impacts need to be represented by parameterizations in atmospheric circulation models (Kim et al. 2003). They also imply that comprehensive measurements of atmospheric gravity waves constitute a tremendous challenge (Alexander et al. 2010): global observations (from satellites) do not have a fine enough resolution to describe the whole spectrum, and measurements with a finer resolution generally provide only a limited spatial coverage. Progress is expected to come from collaborative efforts combining observations and high-resolution modelling, as illustrated by the recent comparisons between observed and modeled gravity waves (Geller et al. 2013).

One of the most significant impacts of gravity waves results from the dynamical forcings they produce in the middle atmosphere (Andrews et al. 1987; Fritts and Alexander 2003): their dissipation induces a convergence of the momentum fluxes (MF) they transport and hence a dynamical forcing. Many studies have focused on quantifying momentum fluxes and describing their geographical and seasonal variations (e.g. Alexander et al. (2008); Ern et al. (2011)), to be compared with their modeled counterparts, parameterized or resolved.

Over the last decade, considerable progress has been made on the observations of the GWs in the lower stratosphere and the middle atmosphere. This progress follows the considerable improvements in satellite measurements (e.g. Ern et al. (2004)) and in their use and interpretation (Alexander 2015), but also from in-situ ballons observations (Vincent et al. 2007; Geller and Gong 2010). These observations, coupled to high resolution simulations reveal that the GW field is more intermittent than anticipated (Hertzog et al. 2008; Alexander et al. 2010), questionning the way

GWs are currently parameterized: having a few intense wave episodes rather than a continuous source with small intensity changes completely the altitudes at which the waves may be expected to dissipate and force the background flow. The probability density function (PDF) of absolute momentum fluxes provides a good means to quantify intermittency and to compare different sources of information on gravity waves (Hertzog et al. 2012), and it is now also used to analyze gravity waves in satellite data (Wright et al. 2013). This intermittency in time and space of the gravity waves can be present in parameterizations that relate the gravity waves to their tropospheric sources. Whereas this is now commonly done for convective gravity waves (using schemes like Beres et al. (2004); Song and Chun (2005); Lott and Guez (2013); Bushell et al. (2015)), this is rather the exception for non-orographic gravity waves parameterizations (Charron and Manzini 2002; Richter et al. 2010). The recent stochastic parameterization of de la Camara and Lott (2015) stands out as having been adapted to incorporate and reproduce this intermittency with a physically based link to the tropospheric flow (Lott et al. 2010, 2012). Nonetheless, there is a pressing need for enhanced understanding of non-orographic gravity waves (Plougonven and Zhang 2014).

The framework and requirements of parameterizations naturally lead us to think in terms of sources, propagation and dissipation as the three successive and distinct stages (or processes) in the life cycle of a gravity wave packet. One would wish to be able to separate each of these processes and relate them to large-scale flow diagnostics. The gravity wave field being generally complex near jets and fronts (e.g. Zhang et al. (2001); Waite and Snyder (2012); Plougonven et al. (2015)), a reasonable aim may be to identify factors in the large scale flow that most efficiently constrain the waves *likely* to be found at a given time and location, rather than seek deterministic relations between the large-scale flow and characteristics of gravity waves that occur at smaller scales.

Based on our investigation of the gravity wave field in several datasets, it has appeared qualitatively that large values of non-orographic GWMF are more likely in regions of strong winds than in regions of weak winds. This is illustrated by two snapshots of the wind speed and GWMF at $z = 20$ km above the Southern Ocean in Figure 1. As expected, the wind speed is a large-scale field, with some small-scale modulations tied to gravity waves. In contrast, the GWMF is patchy, shows very large variations (note the logarithmic color scale) and displays variations on a wide range of spatial scales. Nonetheless, it appears that over ocean regions, the stronger values of GWMF are more likely to be found in regions of strong wind. The present investigation sets out to describe and quantify this relation for the Southern high latitudes in austral spring. It turns out that a simple and robust relation can be found. Its interpretation and use are however not as clear, but we provide an example of use of this relation to critically assess the GWMF parameterized in the parameterization of the LMDz model.

The aim of the present study is to describe and quantify the relation between non-orographic gravity waves and the strength of background stratospheric wind. The metrics used will be the PDFs of the absolute gravity wave momentum flux (GWMF), and the region and season of interest is the Southern polar cap during austral spring. This choice results from the availability of relevant and complementary datasets (see below), but is also motivated by recent studies on the belt of enhanced gravity wave activity observed in the lower stratosphere in austral winter (Hendricks et al. 2014). This belt may be connected to the difficulty of models to describe the breakdown of the polar vortex in spring: it is suspected that this bias comes in part from missing gravity wave drag (McLandress et al. 2012; de la Camara et al. 2016).

The datasets used include mesoscale simulations (Plougonven et al. 2013) and observations collected on superpressure balloon during the Concordiasi campaign (Rabier and coauthors 2010). The simulations have the advantage of providing a wide spatial and temporal coverage. The balloon observations used constitute the most recent and accurate dataset available for gravity waves above the Southern polar cap (Geller et al. 2013). Comparison of these three datasets have been carried out, showing satisfactory agreement (Plougonven et al. 2013; Jewtoukoff et al. 2015), similarly to other comparisons of the resolved gravity waves from the European Center for Medium-range Weather Forecasts (ECMWF) analyses and various observations (Plougonven and Teitelbaum 2003; Wu and Eckermann 2008; Shutts and Vosper 2011).

The paper is organized as follows. Section 2 introduces the data used and methodology. The relation between gravity wave momentum fluxes and the local wind speed is explored in section 3, using PDF conditional on the background wind speed. The processes that may be contributing to this relation are discussed in section 4. Implications, limitations and perspectives are discussed in section 5.

2. Data and methodology

Several datasets are used in order to explore the relation of GWMF to background wind speed:

- mesoscale numerical simulations over the Southern polar cap, run for two months in the Austral spring of 2005 with a resolution of $dx = 20\,\mathrm{km}$;
- analyses of the European Center for Medium-Range Weather Forecasts (ECMWF), for the months of September 2010 to January 2011, corresponding to the Concordiasi campaign. The resolution of the model was T1279, corresponding to a horizontal resolution of 0.125° or about 13 km, with 91 vertical levels corresponding approximately to $500\,\mathrm{m}$ vertical spacing.
- superpressure balloon measurements from the Concordiasi campaign, with the gravity waves analyzed using wavelets and taking advantage of the quasi-Lagrangian behavior of the balloons (Hertzog et al. 2008; Vincent and Hertzog 2014).

The resolution and limitations of each dataset are summarized in table 1. In the mesoscale simulations, no gravity wave parameterization is used. In the ECMWF analyses, only the resolved waves are investigated. In the three datasets, in order to investigate only non-orographic gravity waves, we analyze the gravity wave MF over the oceans and far from islands or coastline (region 5 of Plougonven et al. (2013)).

Before providing more details on these datasets, some explanation on the logic of their choice is necessary. The relation between gravity waves and background winds was found when exploring the mesoscale simulations (Plougonven et al. 2013). The timing and location of these simulations aimed at a comparison with a first balloon campaign (Vorcore, austral spring of 2005) over Antarctica Hertzog et al. (2007). The Concordiasi campaign (austral spring of 2010) was very similar to Vorcore regarding geographical coverage and timing, but the measruements are much improved for gravity wave studies because of enhanced time resolution (every minute instead of every 15 minutes, see 1). As our aim is not a comparison of the balloon measurements to the mesoscale simulations (see Plougonven et al. (2013); Hertzog et al. (2012); Plougonven et al. (2015)), it was logical to use the best available dataset for the balloon observations. The gravity wave momentum fluxes had been analyzed also in the ECMWF analyses (Jewtoukoff et al. 2015), so this readily provided a third, complementary dataset.

The background flow over Antarctica during austral spring is described from the mesoscale simulations (21/10/2005 to 18/12/2005) and from the ECMWF analyses (September to December 2010) in figures 4 and 3. It consists of an upper-tropospheric jet between 40°S and 60°S. It is a region of active baroclinic instability, and is found to be somewhat stronger between 0° and about 120°. In the lower stratosphere, at $z = 20$ km, the flow is dominated by the polar vortex, which is strongest at the end of winter, and breaks up in late spring. The polar vortex is at more poleward latitudes, between 55°S and 75°S. The mean winds in the mesoscale simulations are weaker and show more longitudinal variations, which is mainly due to a shorter time interval and their timing in late spring.

The numerical dataset is derived from mesoscale simulations carried out with the Weather Research and Forecast Model (WRF, Skamarock et al. (2008)), with a domain encompassing Antarctica and the Southern Ocean and for a time period of two months from October 21st to December 18th, 2005. The domain covers an area 10,000×10,000 km wide centered on the South Pole, with a resolution of $dx = 20$ km in the horizontal and 120 levels going up to 5 hPa, see Plougonven et al. (2013) for a complete description. Comparison with balloon observations from the Vorcore campaign (Hertzog et al. 2008) showed good agreement between the simulated and observed momentum fluxes (Plougonven et al. 2013; Hertzog et al. 2012), though both suffered from underestimation because of the limited resolutions.

The balloon measurements used come from the Concordiasi campaign which took place in the austral spring of 2010 (Rabier and coauthors 2010). Long-duration balloons provide one of the most accurate estimates of GWMF (Geller et al. 2013). The temporal resolution of measurements for Concordiasi has been greatly enhanced relative to previous campaigns (measurements every 30s instead of every 15 min), allowing to resolve the full spectrum of gravity waves, hence our choice of this campaign rather than Vorcore (austral spring 2005). The trajectories of the balloons, shown in Figure 2, covered a wide area, part of which is over the Southern Ocean, allowing for the investigation of non-orographic waves. In the balloon observations, the momentum fluxes are estimated using a wavelet analysis: the continuous Morlet wavelet transform applied on the balloon timeseries of pressure, and zonal and meridional winds allows us to locate gravity-wave packets in the time/intrinsic-frequency space, and to estimate phase shifts between these time series. This information, together with the gravity-wave linear theory, are then used to compute momentum fluxes. Note that wavelet coefficients with magnitude smaller than three times the standard deviation of measurement noise are discarded from the statistics. This has probably the detrimental effect of removing some real geophysical signal, but provides confidence that we do not interpret measurement noise as real gravity waves. The reader is referred to Boccara et al. (2008) and Vincent and Hertzog (2014) for further details on how we compute gravity-wave momentum fluxes from the balloon timeseries. These papers also provide estimates of the accuracy with which momentum fluxes are assessed. In particular, Boccara et al. (2008) report that the retrieved gravity-wave momemtum fluxes are underestimated by about 10%, and associated with a $(1-\sigma)$ uncertainty of 10%.

These or similar datasets have been inter-compared previously: the mesoscale simulations have been validated with data from the Vorcore superpressure campaign (Hertzog et al. 2008; Plougonven et al. 2013; Hertzog et al. 2012), and the ECMWF analyses have been shown to contain realistic gravity waves by comparison to the Concordiasi campaign Jewtoukoff et al. (2015). The reader is directed to these earlier studies for an intercomparison of these datasets.

The gravity wave field is characterized by the PDF of the absolute momentum fluxes, $\rho\sqrt{\overline{(u'w')}^2+\overline{(v'w')}^2}$. In the model output, the momentum fluxes are obtained by high-pass filtering spatially the velocity components, see Plougonven et al. (2013) and Jewtoukoff et al. (2015) for further details. As described above, the observed timeseries of momentum fluxes are obtained after a wavelet-based identification of wave packets in the time series of velocity (Boccara et al. 2008; Vincent and Hertzog 2014).

3. Relation between gravity waves and local wind speed

In order to investigate only non-orographic gravity waves, we analyze the gravity wave MF over the oceans (region 5 of Plougonven et al. (2013)). In order to compare with superpressure balloons, the analysis of model output is carried out at $z = 20$ km. This is slightly higher than the flight levels of the balloons (between 17 and 19 km).

a. In different datasets

Gravity wave momentum fluxes in the mesoscale simulations documented by Plougonven et al. (2013) are first investigated. PDFs of absolute momentum fluxes were obtained, using 200 bins that are equally spaced for the logarithm of the GWMF. The PDFs are conditional on the background windspeed $U(x,y,z,t)$ (i.e. simply the total wind speed at that location and time) which was partitionned in intervals of 10 $\mathrm{m\,s^{-1}}$, see Figure 5: for example the green curve corresponds to $p(F\,|\,30 < U < 40\,\mathrm{m\,s^{-1}})$, i.e. the probability to find the value F of the GWMF, knowing that the background wind is between 30 and 40 $\mathrm{m\,s^{-1}}$. Each of these curves, by definition, is normalized such that $\int_0^\infty p(F\,|\,30 < U < 40\,\mathrm{m\,s^{-1}})\,dF = 1$. Finally, note that the vertical axis if logarithmic, to provide detail on the tail of the distributions (rare but intense events which account for a large part of the average GWMF (Hertzog et al. 2012)). Strikingly, the PDFs are found to be very constrained by the background wind, with the frequency of occurence of GWMF larger than 5 mPa systematically increasing with background horizontal wind speed U. For example, values of the GWMF between 35 and 40 mPa are about 100 more likely where the wind is larger than 50$\mathrm{m\,s^{-1}}$ than where the wind is weaker than 10$\mathrm{m\,s^{-1}}$. Note finally that the graphs (semilog in the vertical axis) purposefully emphasize the tails of the PDFs: because of the intermittency of the gravity waves, it is the rare, large events described by the tail of the PDF that matter most (Hertzog et al. 2012). The thin lines in Figure 5 are lognormal approximations of the PDFs, to be discussed in the following subsection.

Figure 6 shows the PDFs of GWMF estimated from the ECMWF analyses, over the same geographical region but for the time of the Concordiasi campaign. Again, strikingly, the PDFs of momentum fluxes are stratified by the background velocity. The values of the momentum fluxes are somewhat larger than those found in the WRF simulations, by a factor 2-3. This is consistent with the expected sensitivity to resolution, whether based on sensitivity tests (Plougonven et al. 2013) or on the truncation of the spectrum of resolved waves (Jewtoukoff et al. 2015).

Figure 7 shows the PDFs of GWMF in balloon observations, conditional on the background wind speed. Relative to Figures 5 and 6, there are surprising similarities and expected differences. The differences include the more irregular nature of the PDFs, expected from a more limited sampling, and the significantly larger values of the GWMF, expected because of the limited resolution of the simulations, see discussion in Jewtoukoff et al. (2015). It is worth stressing that these curves are obtained from *in situ* measurements, that our focus on non-orographic waves induces a limited sampling (see figure 2), and that most of the information is in the tail of the PDFs, i.e. carried by few, rare events. Hence, it is normal that the curves are noisier than the ones obtained from model output. The ordering of the PDFs is not as perfect as for model output, what is striking is rather that, even with such limited sampling, the ordering does come out. The overall picture is again that the tails of the PDFs are generally ordered by the background windspeed, with small exceptions that are compatible with noise due to the limited sampling. Hence the main result we retain is the similarity and confirmation of a strong sensitivity of the PDF to the windspeed. Again, for GWMF values larger than 10 mPa, the curves are generally ordered according to the background wind speed, and the occurrence frequency of large GWMF varies by more than one order of magnitude as a a function of U.

In summary, information on the local wind speed in the lower stratosphere already provides significant information about the GWMF that are likely present. This has been obtained over the ocean for the Southern high latitudes in austral spring. The preference for strong GWMF values to be present in regions of strong windspeeds comes out with striking agreement from the three datasets, whether from observations or from models, and therefore we consider this a very robust result. It is consistent with a well-known aspect of the spatial distribution of GWMF, i.e. the belt of large values found in the stratospheric polar vortex (Hendricks et al. 2014). This belt has been noted in a number of previous studies in time-averaged fields, not from instantaneous values. It has been argued that horizontal propagation and refraction into the jet contributed to this spatial distribution of the gravity waves (Dunkerton 1984; Sato et al. 2009). The present approach sheds a different light on this phenomenology: without reference to geography, it may provide a useful and compact quantification of this preference for large GWMF to be present in regions of strong winds.

Figure 8 shows the medians and the geometric standard deviations in the three datasets, as a function of the background wind speed U. The medians have been normalized for the comparison, whereas the geometric standard deviations naturally are dimensionless (Limpert et al. 2001). For a sample of values following a lognormal distribution with a median F_{50} and a geometric standard deviation $\sigma^* > 1$, 68.2% of the values are expected in the interval $[F_{50}/\sigma^*, F_{50}\,\sigma^*]$, and 95.5% in the interval $[F_{50}/\sigma^{*2}, F_{50}\,\sigma^{*2}]$. The dimensional values of the medians can be found in table 2. Both the values directly calculated from the series of GWMF values (left column) and the values describing the lognormal fits (right column) are displayed. The main, robust conclusion to retain from these panels is that the medians systematically increase with the background wind speed, the increase being surprisingly consistent between the different datasets (factor 3 to 5 between the median for the weakest winds and for the strongest winds). The geometric standard deviations vary significantly from one dataset to another (with the observations in between the two values from the models), but within a dataset they are remarkably insensitive to the background wind speed.

4. Interpretation

The relation highlighted in the previous section appears remarkable because it is robust across several datasets, and because it is simple and can be very succintly summarized (section 3A1 above). In the present section, we try and identify processes that may contribute to this relation, and then further explore this relation in model output and with an offline parameterization, discussing implications for the relevance of the different candidate processes.

a. Candidate processes

Several processes are likely to play a role and contribute to the relation between GWMF and background wind speed:

1. alignment in the vertical of the tropospheric sources and of strong stratospheric winds above: the distribution of sources below may have its maxima coinciding with the polar vortex, with vertical propagation sufficient to yield more intense GWMF in regions of strong winds.

2. Wind filtering: critical levels remove waves with phase velocities matching the wind (Andrews et al. 1987). Regions of strong stratospheric winds may correspond to locations below which there has been less filtering, the strong winds allowing more of the gravity wave spectrum to go through.

3. Lateral propagation of waves: lateral propagation and focusing into the jet is known to occur (Dunkerton 1984; Sato et al. 2009, 2012), and can lead to enhanced GWMF in regions of strong winds.

4. shear as a source of waves: a strong wind speed in the lower stratosphere may oftentimes be associated with strong shear between the troposphere and the stratosphere. Now PV anomalies in shear may act as a source of gravity waves (Lott et al. 2010, 2012).

The different processes outlined above are expected to have different signatures on the relation between GWMF and local windspeed. In the following sections we explore the relation between GWMF and wind speed further, and use those results to discuss the possible relevance of the mechanisms 1-4 outlined above.

b. Variation with altitude

The output of the WRF simulations and of the ECMWF analyses document the relation of GWMF and wind speed at different heights. Figure 9 shows the PDFs of GWMF conditional on the background wind for several heights from the tropopause to the mid-stratosphere. Strikingly, the sensitivity of the PDFs holds at these different altitudes. As expected from previous investigations (e.g. Hertzog et al. (2012)) momentum fluxes decrease with height, and the tails of the PDFs diminish significantly with height. Similar figures were obtained from the ECMWF analyses, at heights of 10, 15, 20 and 30 km. Again, the figures (not shown) are characterized by a robust relation between momentum fluxes and background wind speed at all heights, and the expected decrease of momentum fluxes with height.

In order to determine how the sensitivity of momentum fluxes evolve with height, figure 10 summarizes the variations with background wind speed of the median momentum fluxes, for the different heights and for the two different models. Again, the medians are normalized by the mean of the medians for $20 < U < 30\,\mathrm{m\,s^{-1}}$ and $30 < U < 40\,\mathrm{m\,s^{-1}}$. The two figures are remarkably similar, showing first that the relation is robust and holds at different heights, second that the slope increases a little with height, and third that it deviates from a linear relation at the lowest and highest heights.

Assuming that the sources for momentum fluxes are in the troposphere, the sensitivity of the GWMF PDF to the background wind bears different meanings at different heights: in the lowermost stratosphere, this suggests that the sources are tied to the jet region, which is expected (Plougonven and Zhang 2014). Higher in the stratosphere, and given that larger momentum fluxes in the upper-troposphere are associated with strong winds, it shows that the propagation does not counteract this relation, and in fact somewhat enhances it. Lateral propagation into the regions of stronger winds and critical filtering in regions of weak winds both will tend to enhance the sensitivity of GWMF to U. The present analysis does not allow to conclude on the relative importance of both effects.

If strong stratospheric winds were simply co-located in the vertical with strong upper-tropospheric winds, the PDFs of momentum fluxes in the stratosphere should have the same sensitivity to tropospheric winds as to local wind. Figure 11 illustrates that this is not the case by displaying PDFs of GWMF at 30 km altitude, conditional on the wind speed at 10 km. Although there is still some sensitivity, most of the information has been lost and the differerent PDFs are no longer sorted by knowledge of the wind speed below. This constitutes some evidence for the importance of lateral propagation that has already been emphasized by other means in previous studies (Sato et al. 2012; Senf and Achatz 2011; Ribstein et al. 2015).

Another piece of evidence for lateral propagation comes from the PDF of the orientation of the wave momentum flux relative to the background wind at $z = 20$ km, shown in the upper panel of figure 12. This was obtained from the WRF simulations by calculating the angle, at all locations over the ocean, between the momentum flux vector and the local wind. As seen from figure 4, both the north and south sides of the jet core are sampled in the oceanic region used for the present analysis. Waves are predominantly found to propagate against the flow, i.e. angles between 90 and 270 degrees, and this asymmetry is much more pronounced than at $z = 20$ km (lower panel of figure 12. The difference between the two altitudes is consistent with the expected effect of filtering by the wind. Moreover, there is at $z = 20$ km a strong asymmetry with the mode of the PDF corresponding to an angle of about 225 degrees. Knowing that the winds in the polar vortex are predominantly westerlies, this is indicative of poleward propagation, from source regions located more to the North. Finally, note that this figure is reminiscent of the PDF of the orientation of gravity wave momentum fluxes that was displayed in Plougonven et al. (2015) (their figure 21), but with a somewhat stronger anisotropy.

c. Tropospheric sources

The spatial variations of the gravity wave field is, evidently, in part tied to those of the sources. Nonetheless, this information may be more difficult to capture because non-orographic sources other than convection remain elusive (Plougonven and Zhang 2014) and difficult to quantify. Moreover, as gravity waves ascend in the stratosphere, their propagation modulates the wave field in such a way that the background wind may, on its own, convey more information than the knowledge only of tropospheric sources.

The present section aims at testing whether simple diagnostics that are tied to tropospheric jet/front systems may provide as much information, or more, regarding the gravity wave field than the local wind speed. We restrict our considerations to diagnostics that are simple and very easily available, as was the case for the local wind speed (investigating more sophisticated diagnostics such as the frontogenesis function Charron and Manzini (2002) or the residual of the nonlinear balance equation Zhang et al. (2001) is not the purpose of the present study.) We will consider vorticity, at the surface or in the mid-troposphere, and surface pressure. The former is indicative of fronts, the latter will have a signature at large scales and will point out regions of active cyclogenesis. Other diagnostics could be proposed based on past attempts to parameterize non-orographic gravity waves (Charron and Manzini (2002); Richter et al. (2010) used the frontogenesis function in mid-troposphere) or on idealized and real case studies (O'Sullivan and Dunkerton (1995);

Plougonven et al. (2003); Zhang (2004); Zülicke and Peters (2006, 2008) suggest indicators of imbalance such as Lagrangian Rossby numbers and the residual of the nonlinear balance equation). The range of possibilities is large and its exploration is not the purpose of the present study. The present question is merely: for the region and season of interest, is there a potential source diagnostic, having comparable simplicity to local wind speed, that carries comparable information on GWMF?

Figure 13 shows PDFs of gravity wave momentum fluxes, conditional on different indicators of tropospheric activity. The curves plotted are illustrative: there is very little sensitivity of the PDFs to the underlying vorticity. Similar tests were carried out using the ECMWF analyses, with similar results. In part, this results from the small-scale character of vorticity: even for gravity waves emanating from fronts, they may not show good correlation with the underlying fronts because they propagate away horizontally from the narrow maximum of vorticity which is the signature of the front. This motivated the use of surface pressure, which has signatures on larger scales and for which we expect gravity waves to be enhanced near negative anomalies (extra-tropical cyclones and regions of enhanced precipitation). The PDFs indeed show some sensitivity to this condition on surface pressure, yet the ’stratification’ of the PDFs based on this condition is much weaker than that obtained simply from using the wind at 10 km. Hence another attempt has consisted in using vorticity as a condition, but after having averaged it spatially. Figure 14 shows the PDFs of GWMF again, conditional on the surface vorticity (top) and mid-tropospheric vorticity (bottom) averaged in boxes that are 10 degrees longitude by 5 degrees latitude. The GWMF do show significant sensitivity to the last of these diagnostics, i.e. mid-tropospheric vorticity spatially averaged. This brings support to the choice made by de la Camara and Lott (2015) to use tropospheric vorticity as the indicator for non-orographic, non-convective gravity wave sources. Their motivation for this choice came from theoretical studies of waves emitted by sheared PV anomalies (Lott et al. 2010, 2012).

While it will be of interest to explore further the sensitivity of GWMF to different indicators of the tropospheric flow, the present investigations suffice for the following conclusions: first, the sensitivity of GWMF to the background wind speed in the lower stratosphere is remarkable and it is not straightforward to find a tropospheric diagnostic that carries more, or even comparable, information. Second, possible candidates for such a tropospheric diagnostic include the surface pressure and the mid-tropospheric vorticity (spatially averaged for the latter, as this is a small-scale field).

d. Vertical propagation and parameterizations

It is known that the vertical propagation of waves in the large-scale winds is sufficient to reproduce much of the spatial variability of the gravity wave field (Alexander 1998). As a method to test how much vertical propagation, on its own, can lead to differences in the PDFs of GWMF depending on the backrgound wind, one can use parameterizations from an Atmospheric General Circulation Model (AGCM) run in offline mode. As the near totality of GW parameterizations, the one of LMDz makes the columnar approximation, i.e. gravity waves are assumed to propagate only vertically. Two key advantages of the LMDz parameterization for the present comparison are that it has been designed to describe fluxes that are consistent with observations regarding spectra and intermittency de la Camara et al. (2014), and it includes frontal/jet sources that are physically tied to the resolved tropospheric flow in the model de la Camara and Lott (2015). Following the theoretical arguments of Lott et al. (2010, 2012), the parameterization evaluates the grid-scale vorticity and Richardson number to determine the amplitude of the GWMF emitted, and as a consequence represents the observed GWMF intermittency reasonably well (de la Camara and Lott

2015). Therefore it becomes straightforward, with this parameterization, to produce PDFs of the GWMF conditional on the background wind speed and compare those with the ones obtained above from resolved waves. Input data for the offline runs are daily wind and temperature fields from ERA-Interim for the September 2010 - January 2011 period. Results are shown at 20 km height south of 40°S. Note that the purpose here is to test the effect of vertical propagation and critical filtering (the offline runs are used as a tool to isolate vertical propagation), not to evaluate the most recent version of the constantly evolving parameterization.

Figure 15 shows the PDFs of GWMF conditional on background wind speed in four configurations. The impact of having sources that are physically tied to the tropospheric flow can be seen by comparing the left and right columns: the latter shows results of an offline run of the parameterization where the initial fluxes are set to follow a lognormal distribution, but with no information from the tropospheric flow. With the phase speed spectrum that is used operationally in LMDZ (i.e. a Gaussian distribution of intrinsic phase speeds centered on $0\,\mathrm{m\,s^{-1}}$ with a standard deviation of $40\,\mathrm{m\,s^{-1}}$) the parameterized fluxes that come from homogeneous sources show little sensitivity to the background wind speed. This is probably due to the fact that the change in winds between the launch level and the measurement level is often well below the characteristic value of $40\,\mathrm{m\,s^{-1}}$ used in the parameterization. With the same phase speed spectrum, one can see from the top left panel that the present version of the parameterization (with sources estimated from the tropospheric flow using vorticity (Lott et al. 2010; de la Camara and Lott 2015)) does reproduce part of the sensitivity of the GWMF to the background wind speed. This reflects the collocation of the sources and high wind regions in the upper-troposphere region, as expected from previous sections. With homogeneous sources, it is possible to obtain a sensitivity of GWMF to background wind speed, but this requires a drastic change in the phase speed spectrum (standard deviation of $10\,\mathrm{m\,s^{-1}}$). The sensitivity to the launch level was also investigated, but had little impact. Finally, the effect of reducing the phase speeds in the parameterization with varying sources was tested (lower left panel). Here again, this reduction of the phase speeds allows to obtain a significant dependence of the GWMF to the background wind speed. Note that this dependence remains weaker than that found in the three datasets investigated in section 3. In other words, it appears that specifying the sources from the tropospheric flow accounts for a small part of the relation between GWMF and wind speed. It would be possible to account for a more significant part of this relation by critical filtering and vertical propagation only, but this requires a drastic reduction of the phase speed spectrum, a reduction which seems unrealistic relative to observations (e.g. Jewtoukoff et al. (2015)) and would be an obstacle for the parameterization to fulfill its role in forcing the upper-stratosphere and mesosphere circulation.

5. Summary and conclusion

The relation of non-orographic gravity waves to the background flow has been investigated for waves in the Southern high latitudes in springtime. Several recent observational and numerical studies have emphasized the importance of the intermittency of the gravity wave field (Hertzog et al. 2008; Alexander et al. 2010; Hertzog et al. 2012; Plougonven et al. 2013; Wright et al. 2013) and have proposed PDFs of momentum fluxes as a description of gravity wave momentum fluxes (GWMF) which includes their intermittency. We have investigated the sensitivity of PDFs of GWMF to the local background wind speed, U, in three different and complementary datasets: resolved waves in mesoscale simulations (Plougonven et al. 2013) and in analyses from the ECMWF (Jewtoukoff et al. 2015) and measurements from long-duration balloons of the Concordiasi campaign (Rabier and coauthors 2010). In order to focus on non-orographic gravity waves, only oceanic regions far from orography were considered. It was found that the background wind speed provides significant information on the expected gravity wave MF in this region. The PDF of MF conditional on the background wind speed, U, displayed systematically longer tails and larger medians for larger U (figures 5, 6 and 7). Very good agreement was found between the three very different datasets, providing strong evidence that this is a very robust feature in this region. This relation appears attractively simple, but one should keep in mind that it in only descriptive, i.e. it is not straightforwardly tied to specific processes, as discussed further below.

The present study also confirmed that for non-orographic waves the tails of the PDFs, even for a subset chosen based on background wind values, are very well approximated as lognormal (Hertzog et al. 2012). Hence, the variation of the PDFs of GWMF with respect to the local wind speed was synthesized using their medians and their geometric standard deviation (Limpert et al. 2001). As expected, the medians differ in absolute value (Geller et al. 2013; Jewtoukoff et al. 2015), but their relative variations displayed remarkable consistency between the three datasets. At an altitude of 20 km, the median momentum flux for winds larger than 50 $\mathrm{m\,s^{-1}}$ is about 4 times larger than those for winds weaker than 10 $\mathrm{m\,s^{-1}}$. It is noteworthy that the observational dataset falls in between the two numerical datasets. The geometric standard deviations also differ in value between the different datasets, but they are strikingly insensitive to the background wind speed. For each dataset, they appear as a rather constant parameter for the PDFs of GWMF.

This bias for larger MF in regions of strong winds is consistent with previous results emphasizing a belt of strong gravity wave activity in the stratospheric jet (Ern et al. 2004; Alexander et al. 2010; Sato et al. 2009). Several factors may contribute to this: spatial variations of the tropospheric sources (Hendricks et al. 2014), lateral propagation (Sato et al. 2012), local generation tied to the stratospheric winds (e.g. Sato and Yoshiki (2008)) or the vertical shear (e.g. Lott et al. (2010, 2012)). The relative importance of these different processes was investigated by analyzing the variation with height of GWMF, the relation of GWMF to simple indicators of tropospheric synoptic activity, and by using an offline parameterization (de la Camara and Lott 2015).

At all heights investigated in the outputs of the models between altitudes of 10 and 20 km, the same relation between GWMF and background wind speed was found. Different processes contribute to this, with their relative importance which necessarily varies with height: near the tropopause, the location of sources dominates, whereas effects of propagation should become increasingly important with height. At an altitude of 10 km, a strong sensitivity to local wind was found, implying that the relation above is not purely a result of propagation in the lower stratosphere. The contrast between GWMF in strong winds relative to weak winds increases somewhat with height, indicating that propagation contributes to maintain and even enhance this relation. Nonetheless, this relation is already present at the tropopause level. This reflects that the sources are tied to the upper-tropospheric jet, which is expected. The sensitivity to other diagnostics of the large-scale flow at an altitude of 10 km was also investigated, as a modest attempt to check if a higher level of information on the GWMFs could readily be obtained. Simple tropospheric diagnostics indicative of regions of extra-tropcial cyclones or fronts were used as conditions for the PDFs: surface vorticity, surface pressure, mid-tropospheric vorticity. As the vorticity field has much variability at small scales, it was averaged spatially for a fair comparison. These tests suggest that only the surface pressure and the spatially averaged mid-tropospheric vorticity provided information on the GWMF at 10 km. The sensitivity is at best comparable to that found for local wind. This provides additional justification to the choice of parameterization made by de la Camara and Lott (2015), but further investigation would be required to explore more efficient tropospheric diagnostics.

This latter parameterization (de la Camara and Lott 2015) provides an ideal tool to test the role of vertical propagation and critical level filtering in the relation between GWMF and wind speed: indeed, as the waves are launched stochastically and follow a lognormal distribution, plots similar to the ones obtained from observations and high-resolution models can be produced and compared. By construction, the parameterization only takes into account vertical propagation. The sources can be tied to the tropospheric flow, or they can be made horizontally and temporally homogeneous, so as to isolate the effect of vertical propagation. These tests provide evidence that confirm that the collocation of sources and high-wind regions in the upper-troposphere accounts for part of the relation found at 20 km between GWMF and wind speed, but only for a small part. The tests further show that it is possible to reproduce part of this relation by changing the phase speed spectrum of the waves launched, but that this requires a drastic reduction of the phase speeds (factor 4 relative to what is used successfully in the online version of the parameterization). It is therefore plausible to interpret these results as indirect evidence that variability of the sources and vertical propagation alone can not account for the relation that is found in both observations and numerical models. In other words, this is likely evidence for a missing process, presumably lateral propagation.

Lateral propagation is known to occur (Dunkerton 1984; Sato et al. 2012). Now, this lateral propagation is more pronounced for low-frequency waves than for high-frequency waves (Preusse et al. 2008), and hence one might object that our analysis relies on model output which likely has a bias towards low frequencies for gravity waves Preusse et al. (2014). However, the presence of the relation between GWMF and wind speed in observations from Concordiasi balloons imply that this relation does not apply only to low-frequency waves: whereas the model output (WRF and ECMWF) presumably have a bias towards low-frequency waves because of their limited horizontal resolution, the balloon measurements describe the full spectrum of gravity waves (Jewtoukoff et al. 2015).

Further evidence for lateral propagation stemmed from the investigation of the orientation of the gravity wave momentum fluxes relative to the local wind: the most likely orientation at an altitude of 20 km corresponds to waves propagating against the wind but obliquely (coming from low latitudes and propagating toward the pole). This is consistent with the main source of waves being in the tropospheric storm tracks, which are more equatorward than the poloar night jet, and confirms the lateral propagation already highlighted in the literature (Sato et al. 2009).

The purpose of the present study was to describe the relation of GWMF to diagnostics of the large-scale flow, in the lower-stratosphere. A remarkably robust and simple relation was found between background wind speed and GWMF. It seems attractive because of its compactness and robustness, at least for high Southern latitudes and austral spring. How relevant this relation is for other regions where non-orographic waves are expected to dominate, or at other times, remains an open question. If it is, and is not too sensitive to location and season, it may provide a novel and compact description of the bias for stronger GWMF in regions of strong winds, and become a tool for analyzing gravity waves, complementary to the description of geographical and seasonal variations.

Acknowledgments. The authors acknowledge support from the ANR project StraDyVariUS (Stratospheric Dynamic and Variability, ANR-13-BS06-0011-01). The WRF simulations were performed using HPC resources from GENCI-IDRIS under grants 2012-012039 and 2013-012039. AH and FL benefitted from the SPARC Gravity Wave activity and from ISSI which provided opportunities for exchanges and discussions on these topics. Concordiasi was built by an international scientific group and was supported by the following agencies: Météo-France, CNES, IPEV, PNRA, CNRS/INSU, NSF, UCAR, University of Wyoming, Purdue University, University of Colorado, and ECMWF. AdlC acknowledges support from EMBRACE, and RP is thankful to N. Belabas for useful suggestions. The data used in the present study is available upon request to the corresponding author.

APPENDIX

A1. Lognormal approximation of the tails

The description of the PDF of momentum fluxes highlights the significant weight of rare but intense events. This emphasizes that describing sources of non-orographic gravity waves in parameterizations using a constant value is inappropriate (de la Camara et al. 2014). Now, PDFs of GWMF could well be described by a lognormal distribution (Hertzog et al. 2012). A lognormal distribution is found for a strictly positive variable whose logarithm is normally distributed (e.g. Limpert et al. (2001)). Because the propagation through successive layers of the atmosphere can be seen as a succession of multiplicative reductions of the momentum fluxes, it has been argued that propagation alone could explain the relevance of lognormal distributions (Hertzog et al. 2012). But other reasons, linked to wave sources in the troposphere, may also be relevant. For example, it has been repeatedly highlighted that waves spontaneously generated are exponentially small in Rossby number (Vanneste and Yavneh 2004; Plougonven et al. 2005; Vanneste and Yavneh 2007; Lott et al. 2010). If the distribution of local Rossby number can be roughly described as a Gaussian, the spontaneously emitted waves naturally follow a lognormal distribution (Vanneste, personal communication).

The focus on the tails of the distribution and their presentation in semilog plots may hide the fact that the vast majority of values are wery weak. To illustrate this and clarify how the PDFs are approximated with a lognormal distribution, an example is shown in Figure 16 for momentum fluxes from the WRF simulations over the ocean: the top panel shows a standard plot, emphasizing that the most likely values are close to zero, whereas the bottom panel shows a semilog plot, revealing a shallow tail which extends to large values. Two approximate distributions are overlaid: the lognormal with the same median and geometric standard deviation ($F_{50} = 0.87$ mPa, $\sigma^* = 3.16$), and a lognormal that has been adjusted to better describe the tail ($F_{50} = 0.95$ mPa, $\sigma^* = 3.23$).

The adjustment is carried out using a least squares fit on the logarithms of the distribution, starting from the first percentile. Leaving out the weakest values is justified because they are not the more reliable part of the distribution. In particular the threshold applied during the wavelet analysis of the balloon timeseries may be responsible for an underestimation of the smallest momentum fluxes in this dataset (see Section 2). There was very little sensitivity to the percentile from which we start the fit (first, fifth, tenth...).

Fits to lognormal distributions have been carried out for the three datasets and an illustration is presented in figure 17 for the GWMF in the WRF simulations, which serves to illustrate two points: a minor point is that the PDFs change slowly with height, so that the figure corresponding to a height within the height range of the balloons (17 to 19 km) is very similar to that corresponding to the altitude of 20 km (figure 5). However, the main point to retain from this figure is a confirmation that the tails of the PDFs are well described as lognormal (Hertzog et al. 2012), and the extension of this result to subsets of the GWMF.

References

Alexander, M., 1998: Interpretations of observed climatological patterns in stratospheric gravity wave variance. *J. Geophys. Res.*, **105 (D14)**, 8627–8640.

Alexander, M., 2015: Global an dseasonal variations in three-dimensional gravity wave momentum flux from satellite limb- sounding temperatures. *Geophys. Res. Lett.*, **42**, 6860–6867, doi: 10.1002/2015GL065234.

Alexander, M., and Coauthors, 2008: Global estimates of gravity wave momentum flux from High Resolution Dynamics Limb Sounder Observations. *J. Geophys. Res.*, **113 (D15S18)**, doi:10.1029/2007JD008 807.

Alexander, M., and Coauthors, 2010: Recent developments in gravity-wave effects in climate models and the global distribution of gravity-wave momentum flux from observations and models. *Q.J.R. Meteorol. Soc.*, **136**, 1103–1124.

Andrews, D., J. Holton, and C. Leovy, 1987: *Middle atmosphere dynamics*. Academic Press.

Beres, J., M. Alexander, and J. Holton, 2004: A method of specifying the gravity wave spectrum above convection based on latent heating properties and background wind. *J. Atmos. Sci.*, **61**, 324–337.

Boccara, G., A. Hertzog, R. Vincent, and F. Vial, 2008: Estimation of gravity-wave momentum fluxes and phase speeds from long-duration stratospheric balloon flights. 1. Theory and simulations. *J. Atmos. Sci.*, **65**, 3042–3055.

Bushell, A., N. Butchart, S. Derbyshire, D. Jackson, G. Shutts, S. Vosper, and S. Webster, 2015: Parameterized Gravity Wave Momentum Fluxes from Sources Related to Convection and Large-Scale Precipitation Processes in a Global Atmosphere Model. *J. Atmos. Sci.*, **72**, 4349–4371, doi:10.1175/JAS-D-15-0022.1.

Charron, M., and E. Manzini, 2002: Gravity waves from fronts: parameterization and middle atmosphere response in a general circulation model. *J. Atmos. Sci.*, **59**, 923–941.

de la Camara, A., and F. Lott, 2015: A parameterization of gravity waves emitted by fronts and jets. *Geophys. Res. Lett.*, **42**, 2071–2078, doi:doi:10.1002/2015GL063298.

de la Camara, A., F. Lott, and A. Hertzog, 2014: Intermittency in a stochastic parameterization of nonorographic gravity waves. *J. Geophys. Res. Atmos.*, **119**, 11,905–11,919, doi:10.1002/2014JD022002.

de la Camara, A., F. Lott, V. Jewtoukoff, R. Plougonven, and A. Hertzog, 2016: On the gravity wave forcing during the southern stratospheric final warming in LMDz. *in press for J. Atmos. Sci.*

Dunkerton, T., 1984: Inertia-gravity waves in the stratosphere. *J. Atmos. Sci.*, **41**, 3396–3404.

Ern, M., P. Preusse, M. Alexander, and C. Warner, 2004: Absolute values of gravity wave momentum flux derived from satellite data. *J. Geophys. Res.*, **109 (D20103)**, doi:10.1029/2006JD007 327.

Ern, M., P. Preusse, J. Gille, C. Heppelwhite, M. Mlynczak, J. Russell III, and M. Riese, 2011: Implications for atmospheric dynamics derived from global observations of gravity wave momentum flux in stratosphere and mesosphere. *J. Geophys. Res.*, **116 (D19107)**, doi: 10.1029/2011JD015821.

Fritts, D., and M. Alexander, 2003: Gravity wave dynamics and effects in the middle atmosphere. *Reviews of Geophysics*, **41 (1)**, 1003.

Geller, M., and J. Gong, 2010: Gravity wave kinetic, potential, and vertical fluctuation energies as indicators of different frequency gravity waves. *J. Geophys. Res.*, **115 (D11111)**, doi:10.1029/2009JD012266.

Geller, M., and Coauthors, 2013: A comparison between gravity wave momentum fluxes in observations and climate models. *J. Clim.*, **26**, 6383–6405, doi:10.1175/JCLI-D-12-00545.1.

Hendricks, E., J. Doyle, S. Eckermann, Q. Jiang, and P. Reinecke, 2014: What is the source of the stratospheric gravity wave belt in austral winter. *J. Atmos. Sci.*, **71**, 1583–1592.

Hertzog, A., M. Alexander, and R. Plougonven, 2012: On the probability density functions of gravity waves momentum flux in the stratosphere. *J. Atmosph. Sci.*, **69**, 3433–3448.

Hertzog, A., G. Boccara, R. Vincent, F. Vial, and P. Coquerez, 2008: Estimation of gravity-wave momentum fluxes and phase speeds from long-duration stratospheric balloon flights. 2. Results from the Vorcore campaign in Antarctica. *J. Atmos. Sci.*, **65**, 3056–3070.

Hertzog, A., and Coauthors, 2007: Stratéole/Vorcore - Long duration, superpressure balloons to study the antarctic stratosphere during the 2005 winter. *J. Ocean. Atmos. Tech.*, **24**, 2048–2061.

Jewtoukoff, V., A. Hertzog, R. Plougonven, A. de la Camara, and F. Lott, 2015: Gravity waves in the Southern Hemisphere derived from balloon observations and ECMWF analyses. *J. Atmos. Sci.*, **72**, 3449–3468.

Kim, Y.-J., S. Eckermann, and H.-Y. Chun, 2003: An overview of the past, present and future of gravity-wave drag parametrization for numerical climate and weather prediction models. *Atmosphere-Ocean*, **41**, 65–98.

Limpert, E., W. Stahel, and M. Abbt, 2001: Log-normal distributions across the sciecnes: keys and clues. *BioScience*, **51 (5)**, 341–352.

Lott, F., and L. Guez, 2013: A stochastic parameterization of the gravity waves due to convection and its impact on the equatorial stratosphere. *J. Geophys. Res.*, **118**, 8897–8909.

Lott, F., R. Plougonven, and J. Vanneste, 2010: Gravity waves generated by sheared potential vorticity anomalies. *J. Atmos. Sci.*, **67**, 157–170, doi:10.1175/2009JAS3134.1.

Lott, F., R. Plougonven, and J. Vanneste, 2012: Gravity waves generated by sheared three-dimensional potential vorticity anomalies. *J. Atmos. Sci.*, **69**, 2134–2151.

McLandress, C., T. Shepherd, S. Polaravapu, and S. Beagley, 2012: Is missing orographic gravity wave drag near 60s the cause of the stratospheric zonal wind biases in chemistry-climate models? *J. Atmos. Sci.*, **69**, 802–818.

O'Sullivan, D., and T. Dunkerton, 1995: Generation of inertia-gravity waves in a simulated life cycle of baroclinic instability. *J. Atmos. Sci.*, **52 (21)**, 3695–3716.

Plougonven, R., A. Hertzog, and M. Alexander, 2015: Case studies of non-orographic gravity waves over the Southern Ocean emphasize the role of moisture. *J. Geophysical Research*, **120**, doi:10.1002/2014JD022332.

Plougonven, R., A. Hertzog, and L. Guez, 2013: Gravity waves over Antarctica and the Southern Ocean: consistent momentum fluxes in mesoscale simulations and stratospheric balloon observations. *Quart. J. Roy. Meteorolog. Soc.*, **139**, 101–118.

Plougonven, R., D. Muraki, and C. Snyder, 2005: A baroclinic instability that couples balanced motions and gravity waves. *J. Atmos. Sci.*, **62**, 1545–1559.

Plougonven, R., and H. Teitelbaum, 2003: Comparison of a large-scale inertia-gravity wave as seen in the ECMWF and from radiosondes. *Geophys. Res. Let.*, **30 (18)**, 1954.

Plougonven, R., H. Teitelbaum, and V. Zeitlin, 2003: Inertia-gravity wave generation by the tropospheric mid-latitude jet as given by the fastex radiosoundings. *J. Geophys. Res.*, **108 (D21)**, 4686.

Plougonven, R., and F. Zhang, 2014: Internal gravity waves from atmospheric jets and fronts. *Reviews of Geophysics*, **52**.

Preusse, P., S. Eckermann, and M. Ern, 2008: Transparency of the atmosphere to short horizontal wavelength gravity waves. *J. Geophys. Res.*, **113 (10.1029/2007JD009682)**, D24 104.

Preusse, P., M. Ern, P. Bechtold, S. Eckermann, S. Kalisch, Q. Trinh, and M. Riese, 2014: Characteristics of gravity waves resolved by ECMWF. *Atmos. Chem. Phys.*, **14**, 10 483–10 508, doi:10.5194/acp-14-10483-2014.

Rabier, F., and coauthors, 2010: The Concordiasi project in Antarctica. *Bull. American Meteor. Soc.*, **91 (1)**, 69–86.

Ribstein, B., U. Achatz, and F. Senf, 2015: The interaction between gravity waves and solar tides: Results from 4-d ray tracing coupled to a linear tidal model. *J. Geophys. Res. Space Phys.*, **120**, 6795–6817.

Richter, J., F. Sassi, and R. Garcia, 2010: Toward a physically based gravity wave source parameterization in a general circulation model. *J. Atmos. Sci.*, **67**, 136–156, doi:doi:10.1175/2009JAS3112.1.

Sato, K., S. Tateno, S. Watanabe, and Y. Kawatani, 2012: Gravity wave characteristics in the Southern Hemisphere revealed by a high-resolution middle-atmosphere general circulation model. *J. Atmos. Sci.*, **69**, 1378–1396.

Sato, K., S. Watanabe, Y. Kawatani, Y. Tomikawa, K. Miyazaki, and M. Takayashi, 2009: On the origins of mesospheric gravity waves. *Geophys. Res. Lett.*, **36 (L19801)**, doi:10.1029/2009GL039 908.

Sato, K., and M. Yoshiki, 2008: Gravity wave generation around the polar vortex in the stratosphere revealed by 3-hourly radiosonde observations at Syowa Station. *J. Atmos. Sci.*, **65**, 3719–3735.

Senf, F., and U. Achatz, 2011: On the impact of middle-atmosphere thermal tides on the propagation and dissipation of gravity waves. *J. Geophys. Res.*, **116 (D24110)**, doi:10.1029/2011JD015 794.

Shutts, G., and S. Vosper, 2011: Stratospheric gravity waves revealed in NWP forecast models. *Q.J.R. Meteorol. Soc.*, **137 (655)**, 303–317.

Skamarock, W., and Coauthors, 2008: A description of the Advanced Research WRF Version 3. *NCAR Technical Note*.

Song, I.-S., and H.-Y. Chun, 2005: Momentum flux spectrum of convectively forced internal gravity waves and its application to gravity wave drag parameterization. Part I: Theory. *J. Atmos. Sci.*, **62**, 107–124.

Vanneste, J., and I. Yavneh, 2004: Exponentially small inertia-gravity waves and the breakdown of quasi-geostrophic balance. *J. Atmos. Sci.*, **61**, 211–223.

Vanneste, J., and I. Yavneh, 2007: Unbalanced instabilities of rapidly rotating stratified shear flows. *J. Fluid Mech.*, **584**, 373–396.

Vincent, R., and A. Hertzog, 2014: The response of superpressure balloons to gravity wave motions. *Atmospheric Measurement Techniques*, **7 (4)**, 1043–1055.

Vincent, R., A. Hertzog, G. Boccara, and F. Vial, 2007: Quasi-Lagrangian superpressure balloon measurements of gravity-wave momentum fluxes in the polar stratosphere of both hemispheres. *Geophys. Res. Lett.*, **34 (L19804)**, doi:doi:10.1029/2007GL031072.

Waite, M. L., and C. Snyder, 2012: Mesoscale energy spectra of moist baroclinic waves. *J. Atmos. Sci.*, **70 (4)**, 1242–1256.

Wright, C., S. Osprey, and J. Gille, 2013: Global observations of gravity wave intermittency and its impact on the observed momentum flux morphology. *J. Geophys. Res.*, **118**, 10,98010,993, doi:10.1002/jgrd.50869.

Wu, D., and S. Eckermann, 2008: Global gravity wave variances from Aura MLS: characteristics and interpretation. *J. Atmos. Sci.*, **65 (12)**, 3695–3718.

Zhang, F., 2004: Generation of mesoscale gravity waves in upper-tropospheric jet-front systems. *J. Atmos. Sci.*, **61 (4)**, 440–457.

Zhang, F., S. Koch, C. Davis, and M. Kaplan, 2001: Wavelet analysis and the governing dynamics of a large amplitude mesoscale gravity wave event along the east coast of the united states. *Q.J.R. Meteorol. Soc.*, **127**, 2209–2245.

Zülicke, C., and D. Peters, 2006: Simulation of inertia-gravity waves in a poleward breaking Rossby wave. *J. Atmos. Sci.*, **63**, 3253–3276.

Zülicke, C., and D. Peters, 2008: Parameterization of strong stratospheric inertiagravity waves forced by poleward-breaking rossby waves. *Mon. Wea. Rev.*, **136**, 98–119.

LIST OF TABLES

Dataset	Resolution	Observed waves
WRF simulations	$dx = 20$ km, dz 300 m	$\lambda_h > 120$ km, $\lambda_z > 2$ km
ECMWF analyses	dx 13 km, dz 500 m	$\lambda_h > 80$ km, $\lambda_z > 3$ km
Concordiasi balloons	Measurements every minute	Whole spectrum: $f < \hat{\omega} < N$.

TABLE 1. Summary of the resolution and expected limitations of the three datasets used to diagnose the relation between gravity waves and background wind speed. The last column provides an estimate of the horizontal wavelength (λ_h) and vertical wavelength (λ_h) that can confidently be resolved.

U, in $\mathrm{m\,s^{-1}}$	$[10,20]$	$[10,20]$	$[20,30]$	$[30,40]$	$[40,50]$	$50 < \ldots$
WRF, medians (mPa)	0.18	0.24	0.36	0.48	0.59	0.87
gsd	3.2	3.2	3.3	3.3	3.3	3.2
ECMWF, medians (mPa)	0.43	0.60	0.73	0.91	1.13	1.30
gsd	4.4	4.2	4.5	4.7	4.8	4.7
Balloons, medians (mPa)	2.56	4.00	4.95	6.28	8.24	10.8
gsd	2.1	1.9	1.9	1.9	2.0	1.9

TABLE 2. Characteristics of the PDFs of the GWMF from the three datasets, in each of the wind speed intervals. Medians are indicated in mPa, geometric standard deviations (gsd) are dimensionless.

LIST OF FIGURES

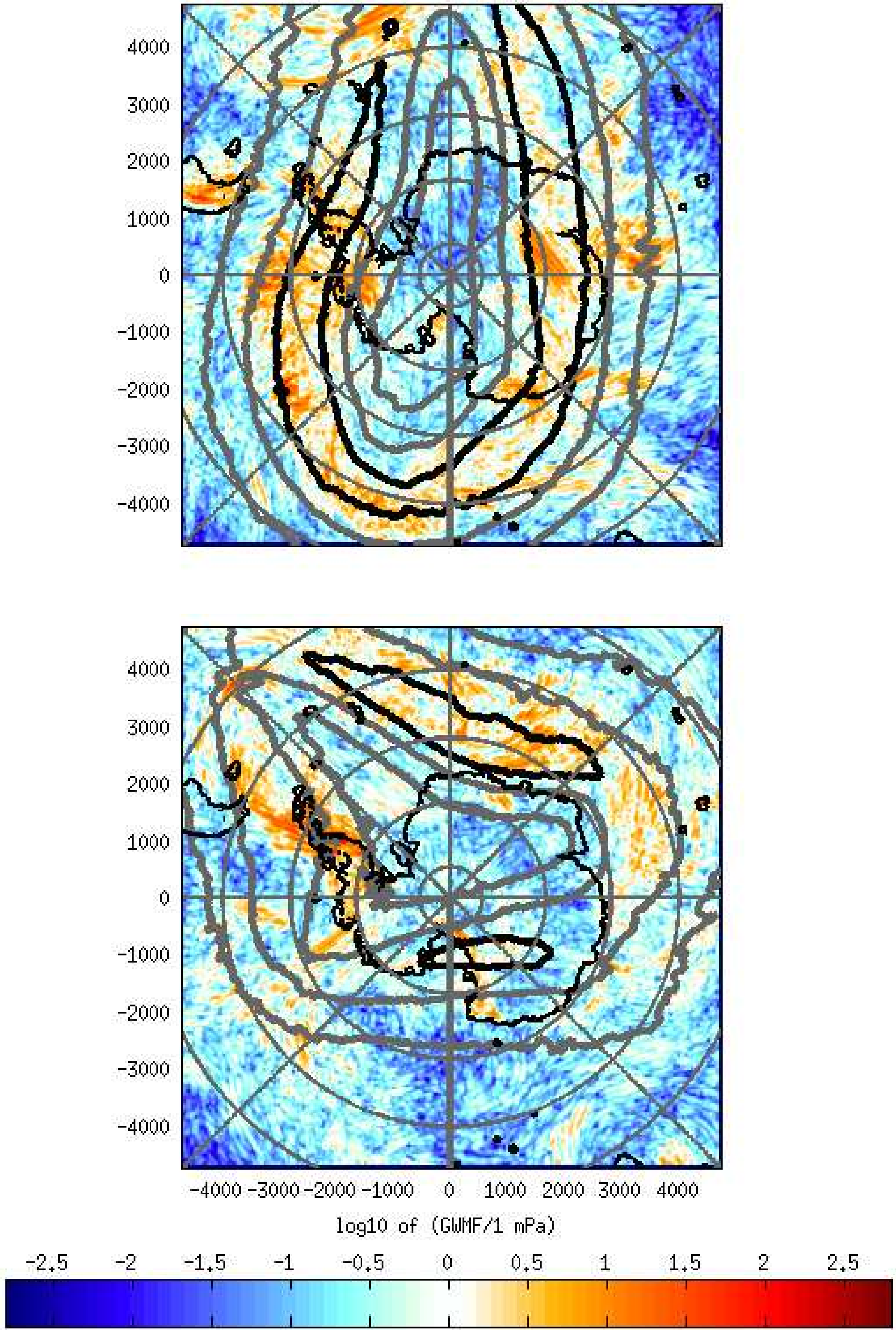

FIG. 1. Two examples of snapshots of absolute momentum fluxes (colors, logarithmic scale) and wind speed (thick gray lines for isotachs 20 and 40 $\mathrm{m\,s^{-1}}$, thick black line for 60 $\mathrm{m\,s^{-1}}$) at an altitude of $z = 20$ km, from the mesoscale simulations of the flow above Antarctica and the Southern Ocean (Plougonven et al. 2013). The dates are October 23rd, 18:00UTC for the top panel, November 7th, 2005, 12:00UTC for the bottom panel.

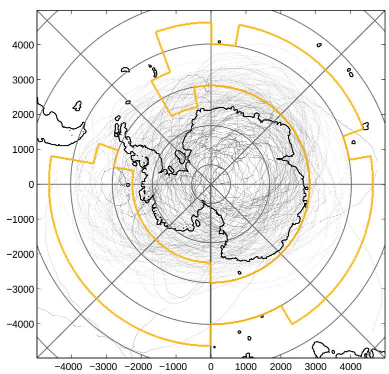

FIG. 2. Trajectories of the nineteen Concordiasi balloons above Antarctica and hte Southern Ocean (gray points, one every 12 hours), along with the outline (thick orange line) of the non-orographic region used for the analysis of the three datasets (region 5 from Plougonven et al. (2013)).

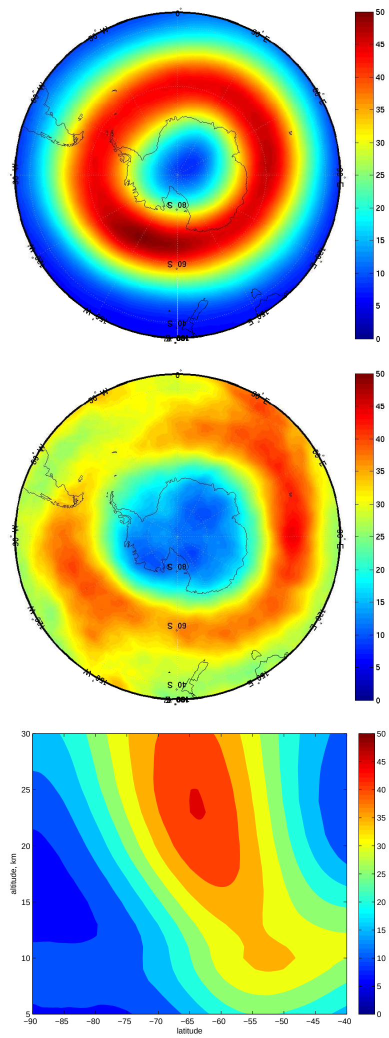

FIG. 3. Winds averaged from September to December 2010, from the analyses of the ECMWF, described by horizontal maps at $z = 20$ km (top), at $z = 10$ km (middle) and by a vertical cross-section (bottom). Note that the colorbars are adapted to each panel.

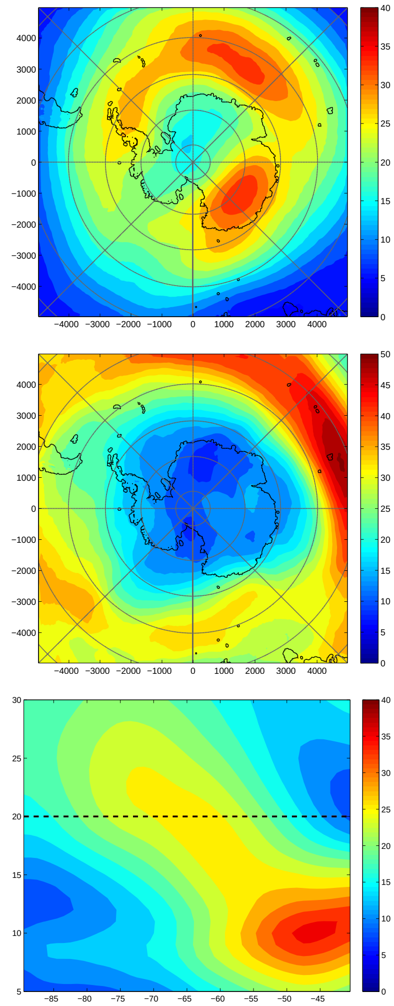

FIG. 4. Winds averaged from October 21st, 2005, to December 18th, 2005, from the WRF simulations. Panels are as in figure 3.

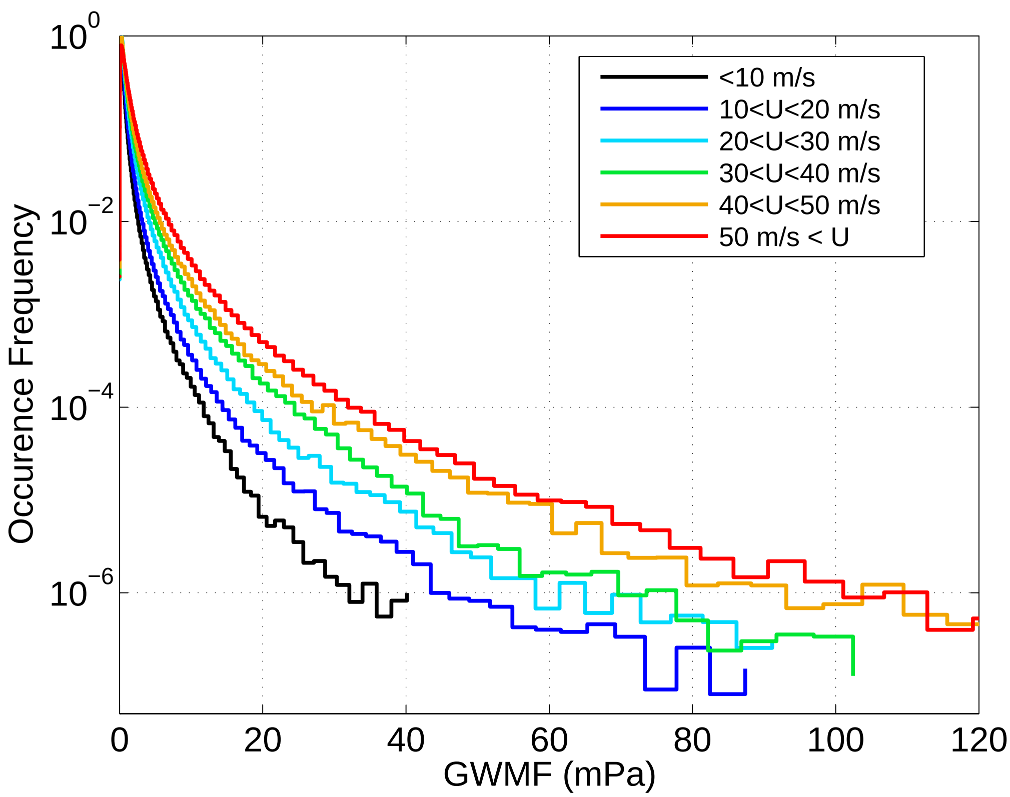

814 FIG. 5. Probability Density Functions of the gravity wave momentum fluxes (GWMF) in mPa from the WRF
815 simulations, at $z = 20\,\text{km}$, conditional on the background wind.

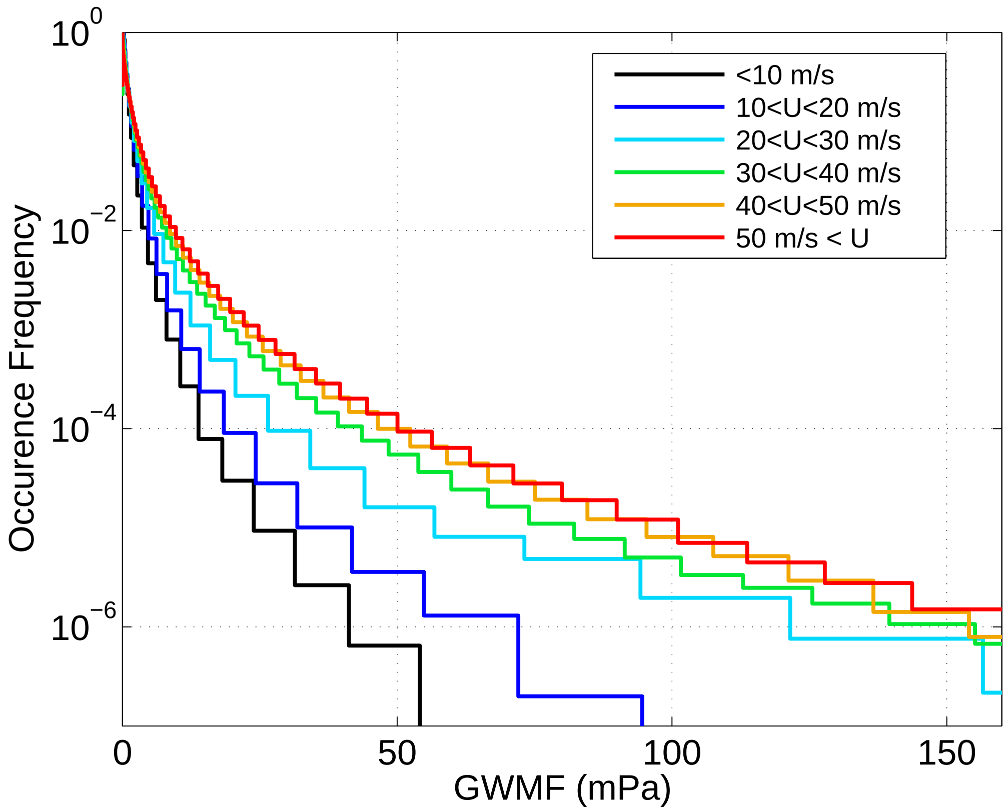

816 FIG. 6. Same as Figure 5 but for the momentum fluxes calculated from the ECMWF analyses, for the time of
817 the Concordiasi campaign, September 2010 to January 2011.

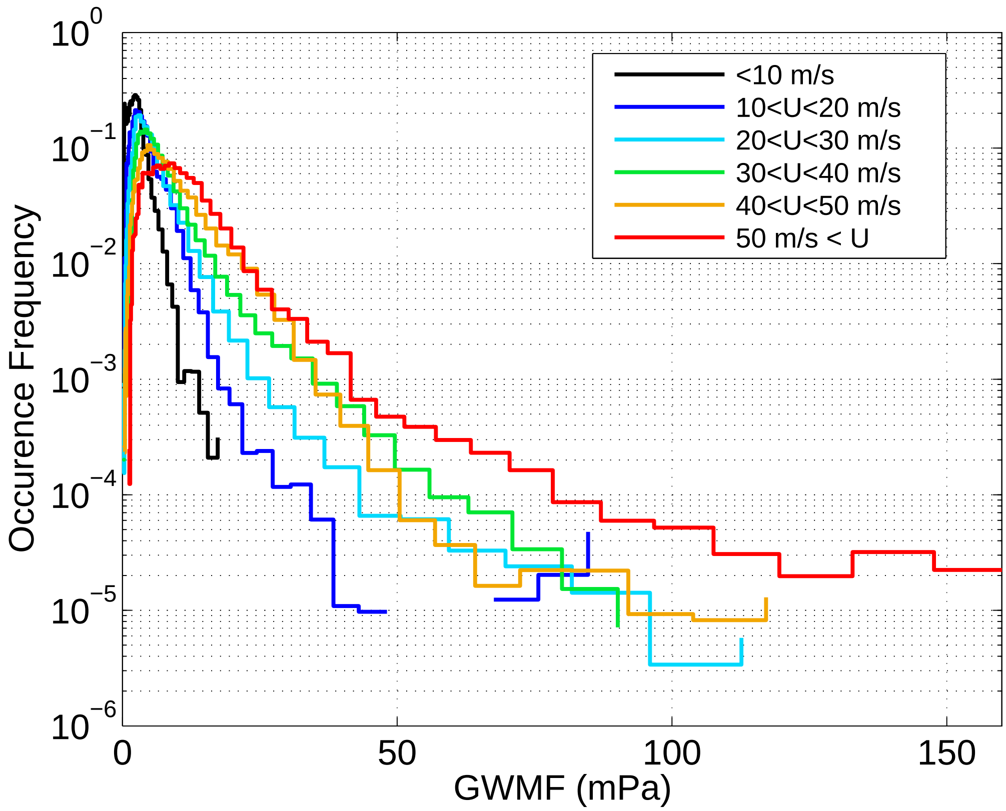

818 FIG. 7. Same as Figure 5 but for the long-duration balloons of the Concordiasi campaign, September 2010 to
819 January 2011.

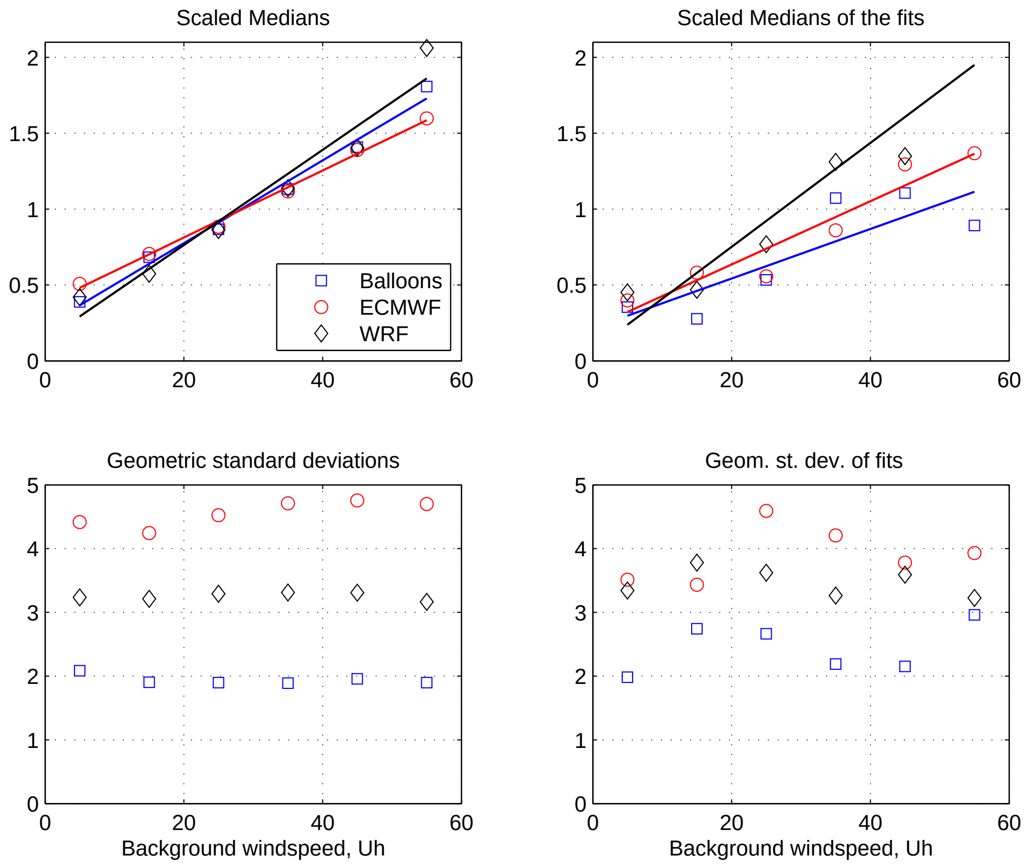

820 FIG. 8. Normalized medians of the PDFs of GWMF (top) and geometric standard deviations (bottom) as a
821 function of the background wind speed. Black symbols correspond to the mesoscale simulations, red symbols to
822 the ECMWF output, and blue symbols to the Concordiasi balloons. The medians were normalized by the means
823 of the medians found for winds between 20 and 40 $\mathrm{m\,s^{-1}}$. For the medians, the linear regressions (thin lines) are
824 also displayed.

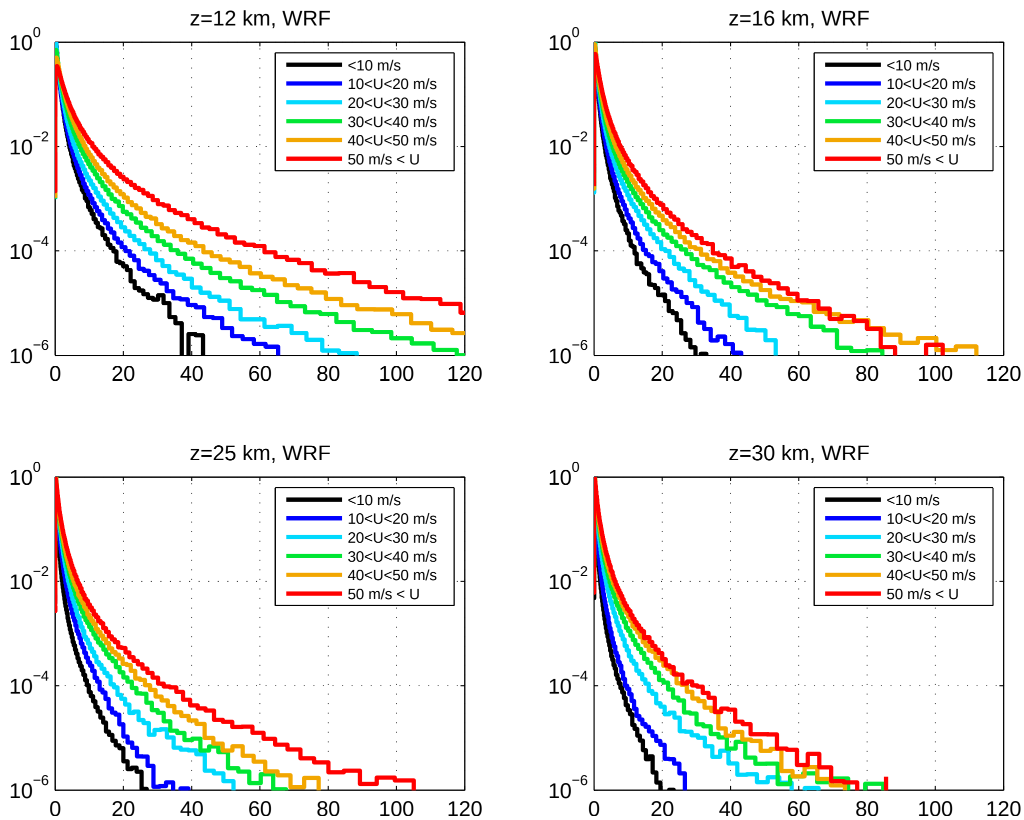

FIG. 9. PDFs of momentum fluxes conditional on the background wind speed at four different heights in the WRF simulations: $z = 12$ km (upper-left), $z = 16$ km (upper-right), $z = 25$ km (lower-left) and $z = 30$ km (lower-right). .

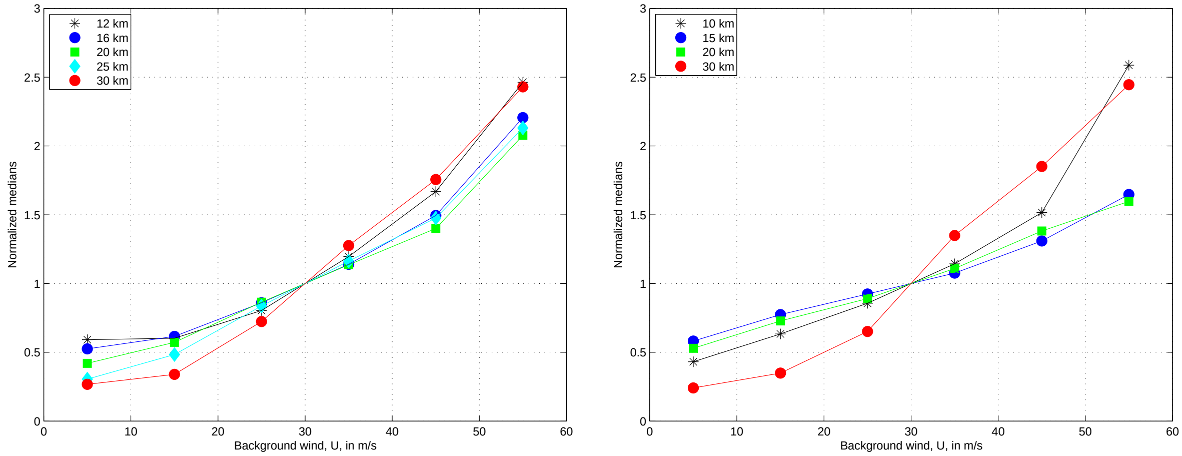

FIG. 10. Variation of the normalized median of GWMF with background wind speed U, from the WRF simulations (left) and the ECMWF analyses (right) for different heights (see legend in each graph).

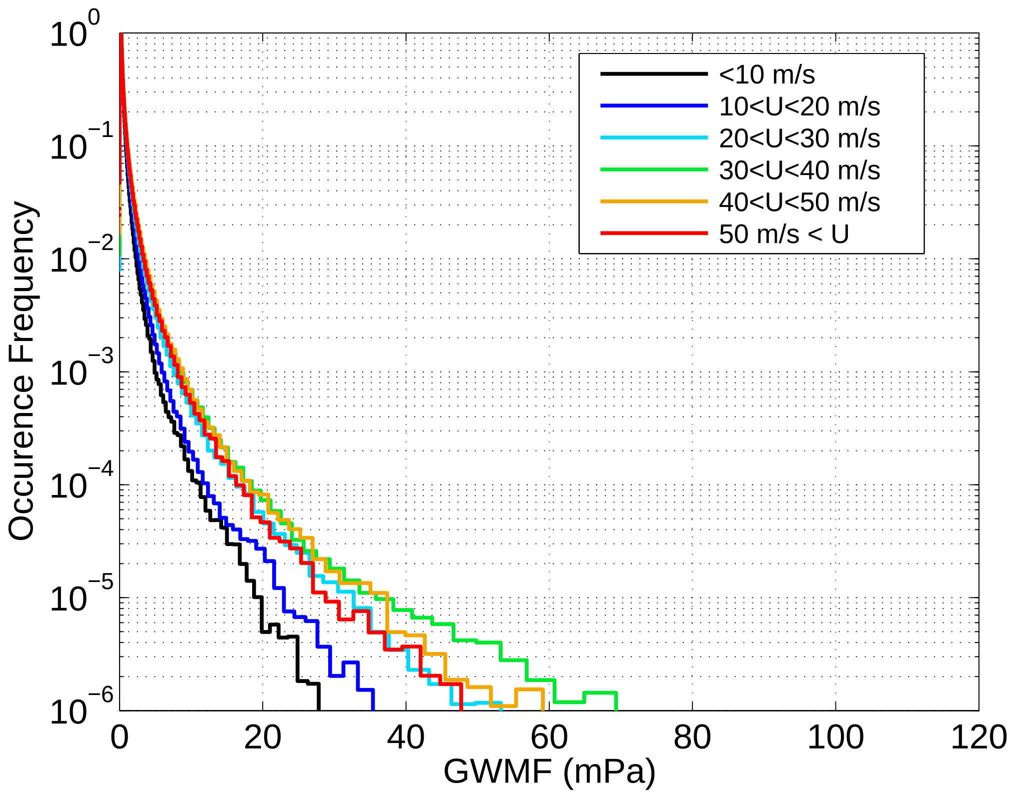

FIG. 11. PDFs of gravity wave momentum fluxes at 30 km, in the WRF simulations, conditional on the wind speed at 10 km.

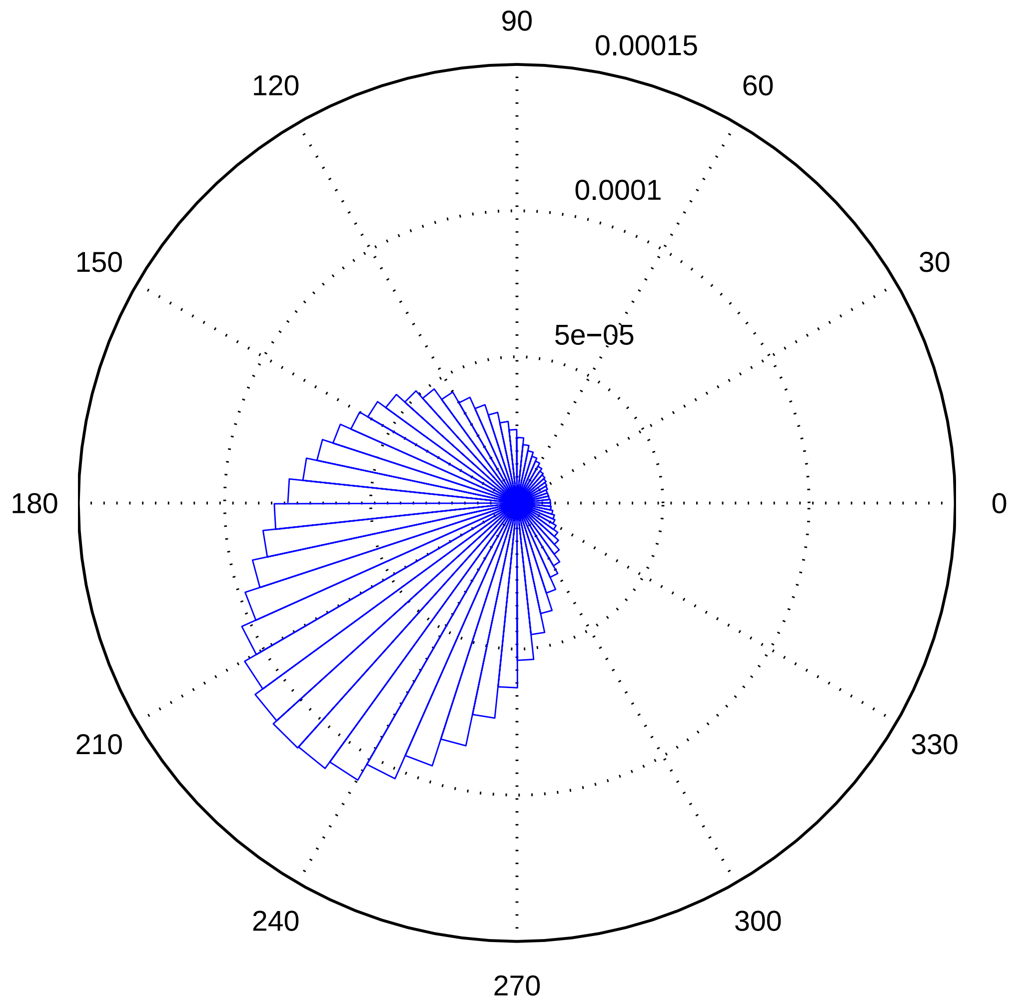
90
0.00015
120
60
0.0001
150
30
5e−05
180
0
210
330
240
300
270

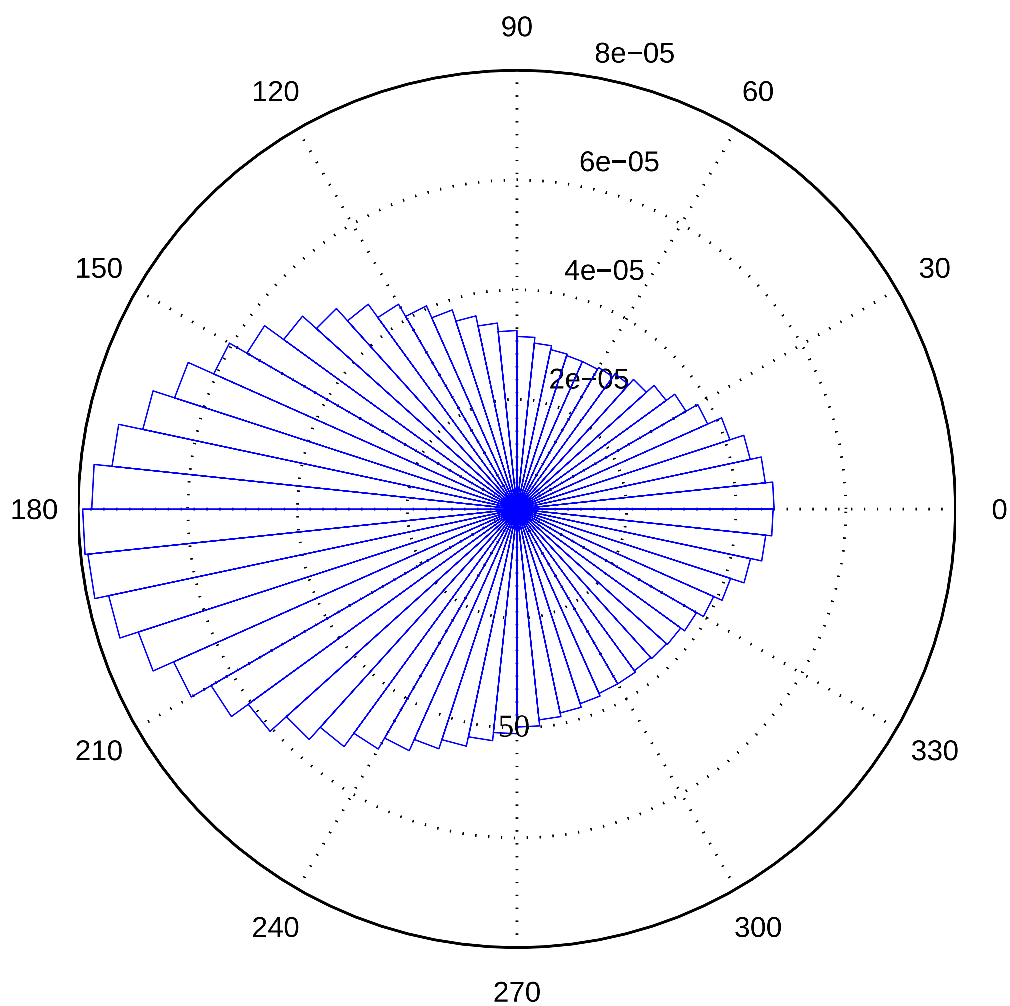
90
8e−05
120
60
6e−05
150
30
4e−05
2e−05
180
0
50
210
330
240
300
270

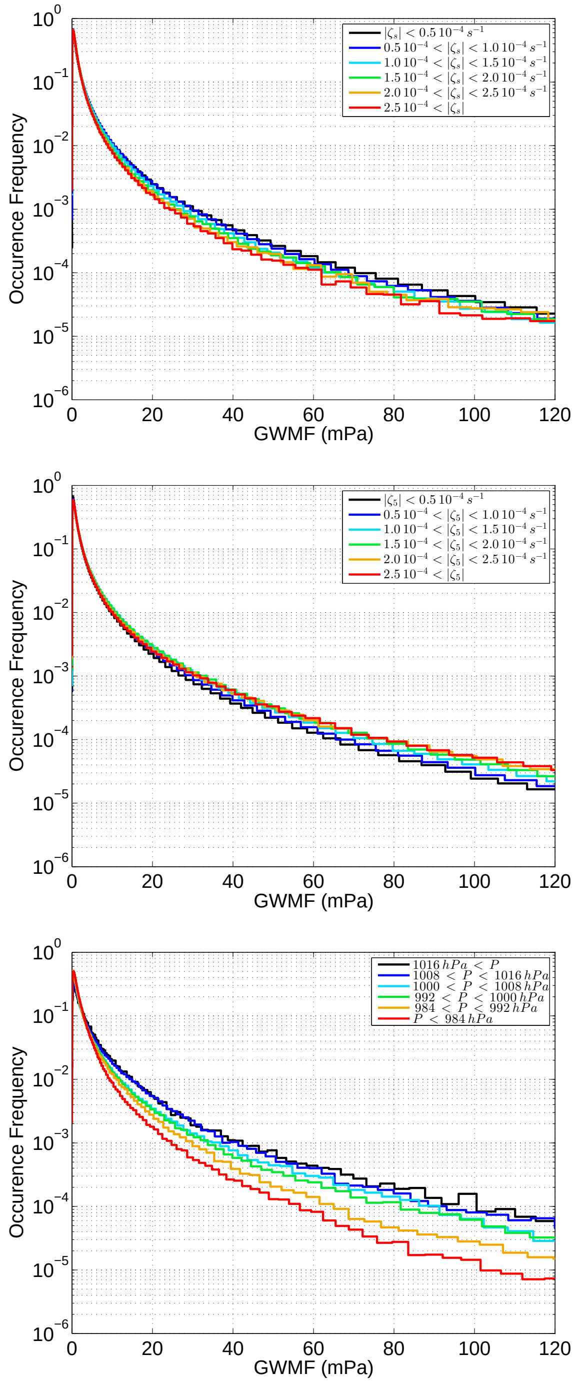

FIG. 13. PDFs of GWMF at $z = 10\,\text{km}$ conditional on different indicators of tropospheric jet/front activity. First panel: conditional on the absolute value of surface vorticity, by increments of $0.5\,10^{-4}\,\text{s}^{-1}$. Second panel: conditional on the absolute value of relative vorticity at $z = 5\,\text{km}$, by increments of $0.5\,10^{-4}\,\text{s}^{-1}$. Third panel: conditional on surface pressure anomaly, sorted by increments of 10 hPa.

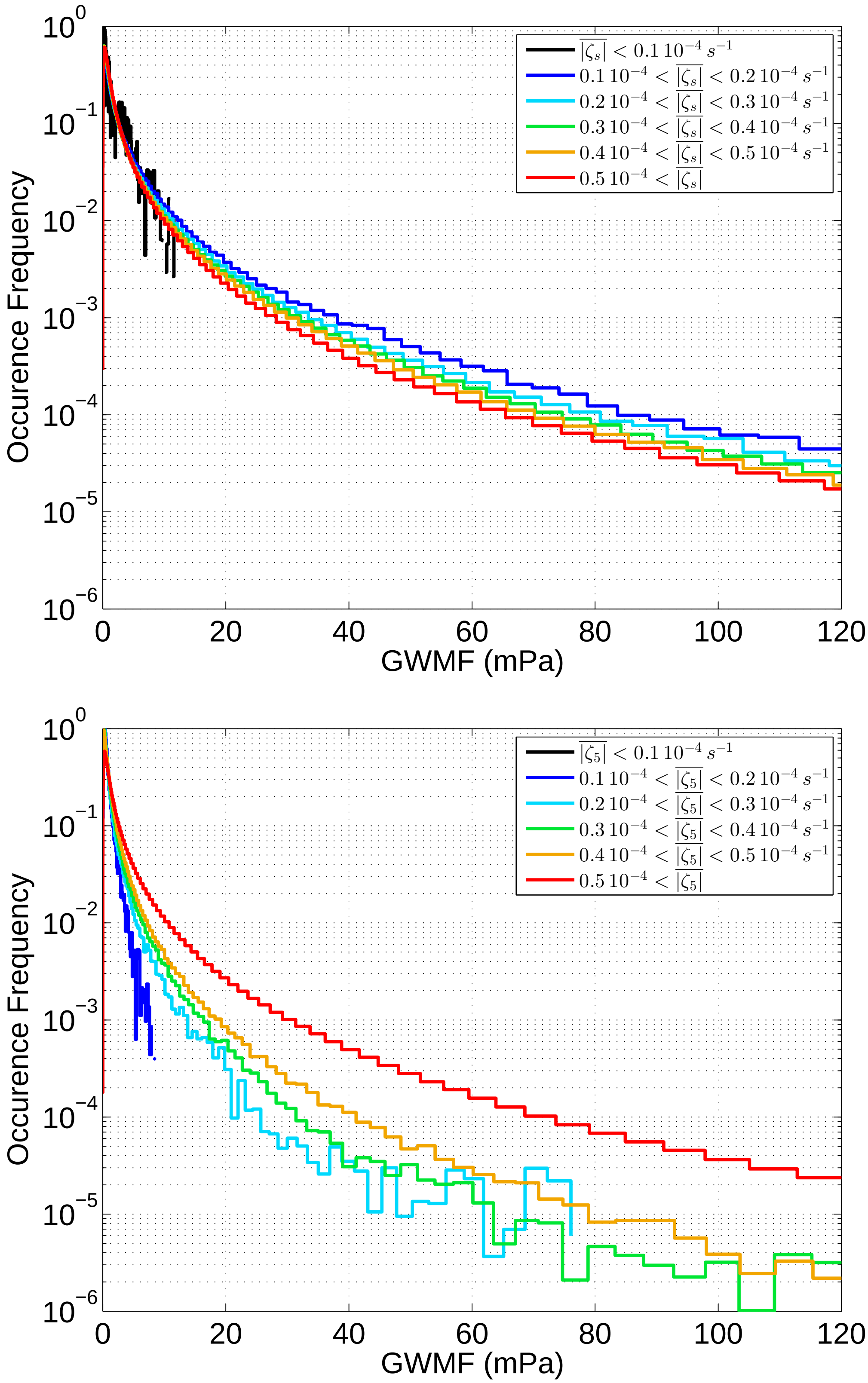

FIG. 14. PDFs of GWMF conditional on the absolute values of relative vorticity at the surface (top) and at the mid-troposphere (bottom), averaged in boxes that are 10 degrees longitude by 5 degrees latitude.

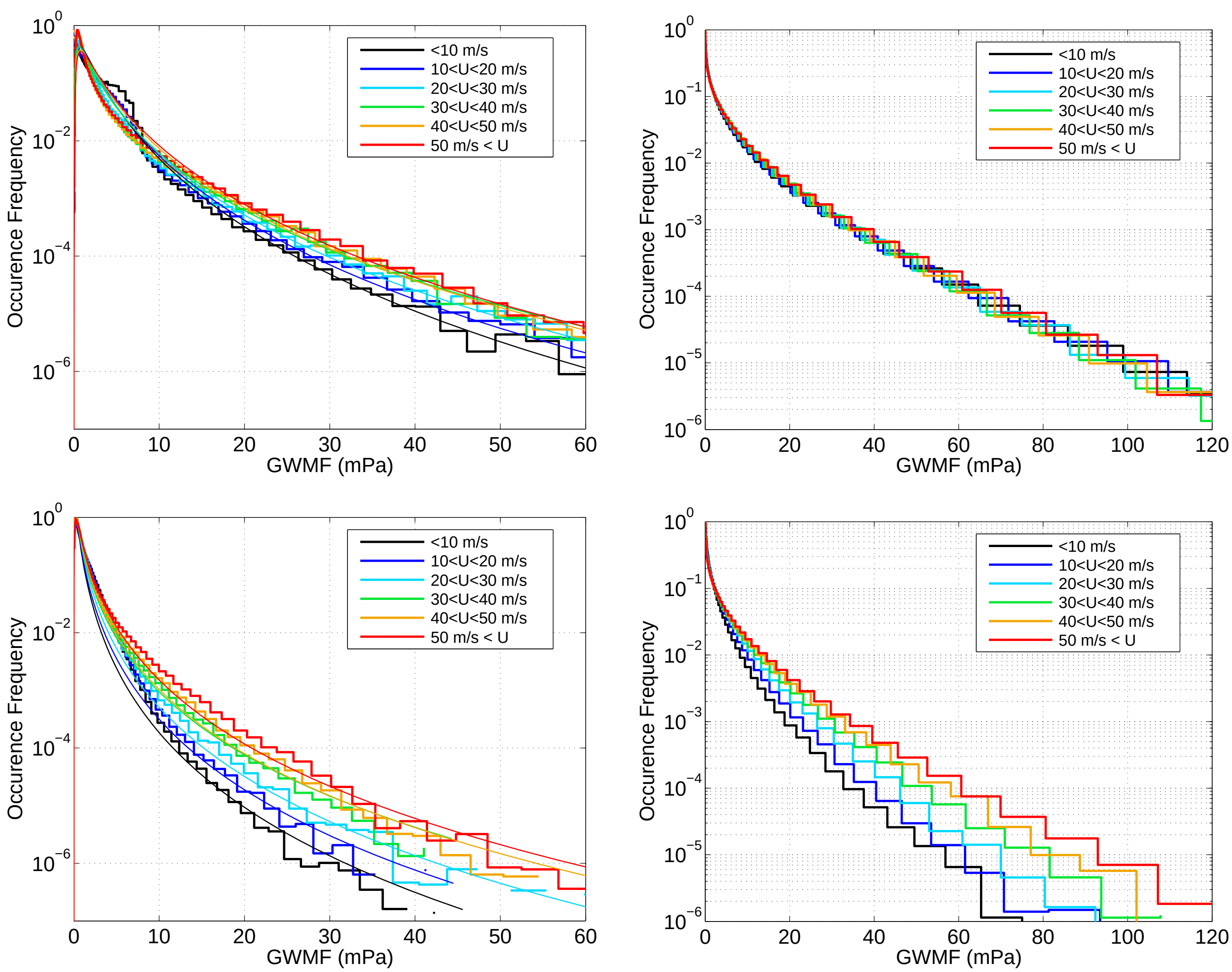

FIG. 15. PDFs of the parameterized GWMF, using the parameterization of the LMDz Atmospheric General Circulation Model. The scheme is used offline, for the period from September 2010 to January 2011. The left column shows results for the parameterization used with the source varying with the tropospheric flow (see de la Camara and Lott (2015) for details). The right column shows results using a source which retains a lognormal distribution but with the amplitudes independent of the tropospheric flow. The standard deviations for the phase speeds are 40 $\mathrm{m\,s^{-1}}$ for the upper panels, and 10 $\mathrm{m\,s^{-1}}$ for the lower panels.

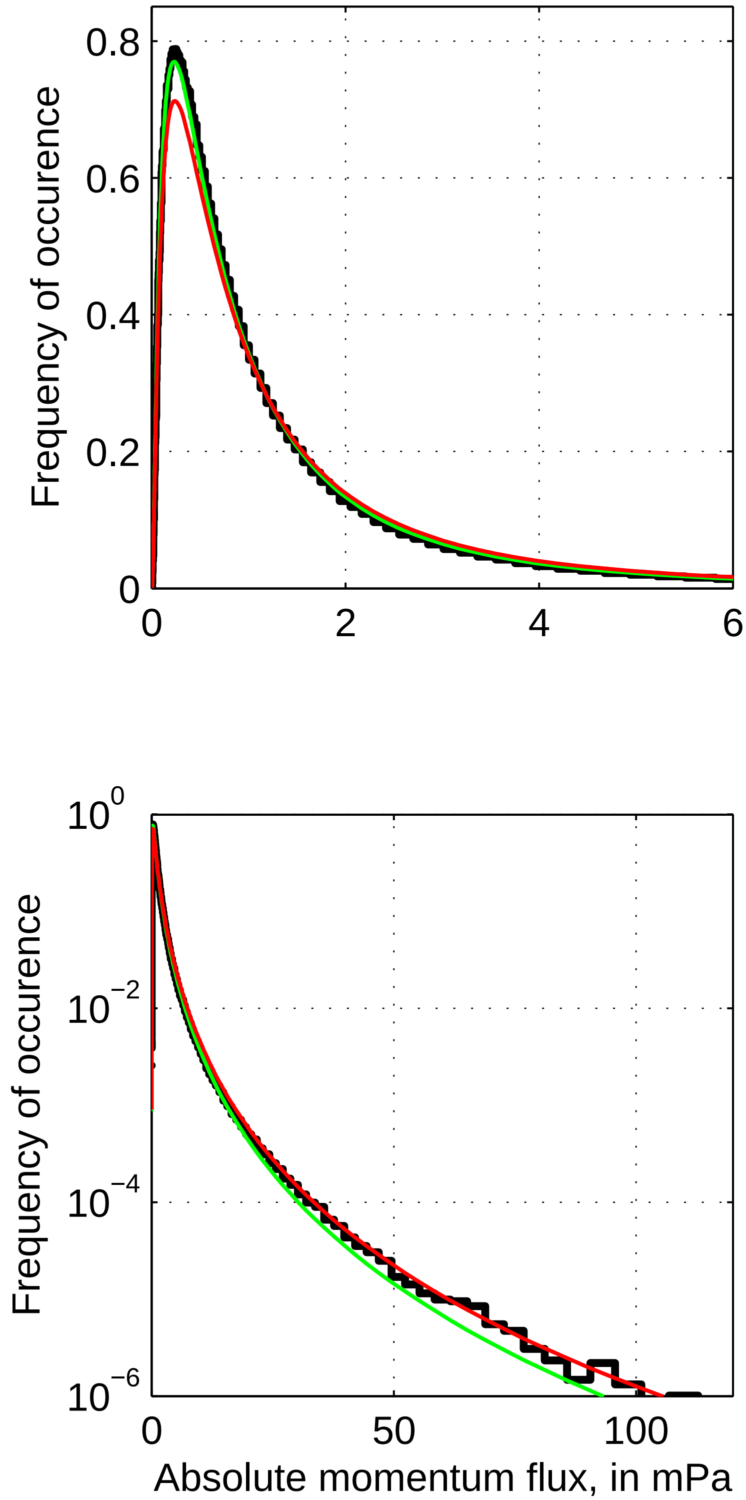

FIG. 16. Example of the fit using a lognormal, for the PDF of momentum fluxes found over the ocean at $z = 20$ km in the WRF simulations, for background winds larger than 50 m s^{-1}. Three lines are shown: the thick black line is for the PDF estimated using 200 bins equally spaced for the logarithm of momentum fluxes, the thin green line depicts the lognormal PDF with the same median and geometric standard deviation, the red line is the optimized lognormal PDF. Top panel: standard plot of the PDF, showing the emphasis of values near zero (horizontal axis only extends to 6 mPa). Bottom panel: semilog view of the complete distribution.

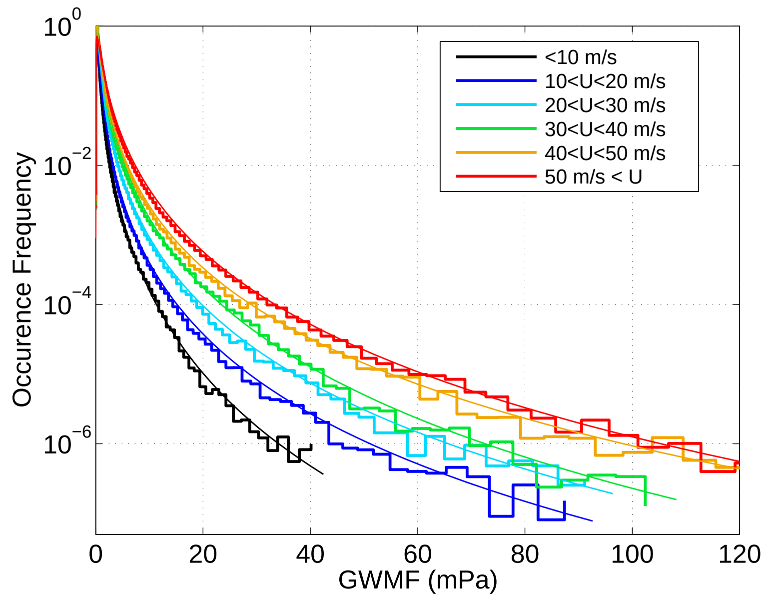

852 FIG. 17. PDFs of GWMF at a height of 18 km, from the WRF simulations. Also shown, as thin lines, are the
853 the lognormal distributions fitted to approximate their tails, as described in the text.